Hindawi
Mathematical Problems in Engineering
Volume 2022, Article ID 5816393, 21 pages
https://doi.org/10.1155/2022/5816393

Research Article

Studying the Applicability of Swarm Intelligence in Designing Optimized PI Controller for DC-DC Zeta Converter: A MATLAB-Based Approach

Md. Rafid Kaysar Shagor, Samiur Rahman Sami, Mirza Muntasir Nishat, Fahim Faisal, Md. Safwan Zaman, and Zubayer Ahmed

Department of EEE, Islamic University of Technology, Gazipur, Bangladesh

Correspondence should be addressed to Mirza Muntasir Nishat; mirzamuntasir@iut-dhaka.edu

Received 14 May 2022; Accepted 1 September 2022; Published 28 September 2022

Academic Editor: Laxminarayan Sahoo

Studying the stability of power converters and improving the performance is a major concern for researchers in the domain of power electronics. In this context, the DC-DC Zeta converter is studied in this paper and the closed-loop operation is comprehensively investigated by employing swarm intelligence (SI) algorithms with a view to design an optimized proportional-integral (PI) controller. These algorithms have been increasingly used to develop and optimize power converters in recent years. The state-space averaging technique was used to design the converter's closed-loop transfer function. Hence, the traditional and SI algorithm-based PI controllers are inspected, and comparative analysis is presented. Four objective functions termed as integral absolute error, integral time absolute error, integral square error, integral time squared error, gain values, and different performance parameters such as percentage of overshoot, rise time, settling time, and peak amplitude are tabulated to examine the stability of the system. Furthermore, eigenvalues have been analyzed for determining the stability of the system extensively. Finally, a detailed comparative study is shown to provide a detailed evaluation of the performances where ant colony optimization for continuous domains (ACOR)-based PI controller has shown promising results than other SI-based controllers in terms of percentage of overshoot (2.27%), rise time (1.54 μs), and settling time (0.103 μs). All the simulation results and analysis are obtained using the MATLAB-Simulink.

1. Introduction

In this modern era of technology, designing sophisticated power electronic devices carries immense importance in the research community. This emerging technology has made its way into various applications, including renewable energy generation, electric vehicle (EV), biomedical equipment, and tiny appliances like laptop and mobile phone chargers, LED drives, microgrid systems. [1]. In this regard, DC-DC converters are the simplest basic electronic circuits for converting DC voltage switching activity [2]. Apart from turning the source's DC output into a regulated DC voltage, the DC-DC power converter also performs handful significant control duties. For example, it can track the maximum power point (MPPT) for different renewable sources [3]. Buck, Boost, Buck-Boost, Cuk, SEPIC, Zeta, and other advanced DC-DC converters are all examples of DC-DC converters. Buck, Boost, and Buck-boost can perform step down, step up, and step up-down actions, respectively. However, some higher order converters like Zeta, Cuk, and SEPIC converters, allow power when the demand required a low input voltage and a high output voltage [4–9]. In correlation with Cuk and SEPIC converters, the Zeta converter is a nonlinear, noninverting fourth-order converter that can operate as buck-boost-buck with respect to input and boost-buck-boost with respect to energy output. The key advantages of the Zeta converter are reduced switching stress, flexibility, and nonpulsating output current. It is dependent on the duty cycle, which can be operated in several modes such as boost and buck [10]. In addition, Zeta outperforms

SEPIC in terms of maintaining a stable feedback loop for a more comprehensive input voltage range, higher load transients, reduced output voltage ripple, and simpler compensation [11]. However, an open-loop Zeta converter cannot meet expectations based on the performance characteristics of the percentage of overshoot, rise time, settling time, and peak amplitude. As a result, a controller is required to improve performance and keep the output voltage stable.

For decades, the PI controller has been one of the most basic and extensively used controllers as it uses a control loop feedback mechanism to control process variables. A proportional parameter (Kp) will lower the rising time and the steady-state error but never completely removes it. On the other hand, integral feedback (Ki) can be used to eliminate the steady-state error and lower the amount of forwarding gain required. The goal of a typical PI tuning controller technique is to get the performance index under consideration to a minimum or maximum value. However, it is challenging to identify appropriate values for Kp and Ki in a simple PI tuner by manual tuning method for proper control. In this context, different forms of smart and intelligence algorithms can be brought into action to make the whole system automated and more sophisticated. For instance, swarm intelligent (SI) algorithms have received notable attention from the power and control engineers in this regard. The potential parallelism and distributed properties of SI algorithms allow them to solve difficult nonlinear problems with enhanced capabilities in terms of self-adaptability, resilience, and searchability [12]. Among different SI-based optimization methods, particle swarm optimization (PSO), artificial bee colony (ABC), firefly algorithm (FA), shuffled frog leaping algorithm (SFLA), ant colony optimization for continuous domain (ACOR), and chimp optimization technique [13–19] are employed by different researches in various times in a wide range of power electronics-based application. In [20], the output regulation of the Zeta converter was addressed in the presence of model uncertainty, input voltage changes, and load variations. The linear matrix inequality tool was used to construct and solve this problem, resulting in an optimal robust state feedback controller. Finally, the performance of the proposed method was compared to the traditional PI controller. In [21], an ACOR-based PID controller was presented for the Zeta converter with the model order reduction method. The SSA technique was utilized to obtain the linear model of the Zeta converter, and the fourth-order transfer function was derived in terms of the duty ratio to the output voltage. On the other hand, the study in [22] displayed the analysis and design of a DC-DC Buck converter with a cascaded control strategy by employing PSO and gravitational search algorithm (GSA) adjusted PI and slide mode controller (SMC). In [23], an ABC-PID controller algorithm was designed and implemented in a buck converter. In terms of settling time, steady-state error, and load change scenarios, the results reveal that ABC-PID outperforms genetic algorithm (GA)-based PID in controller. However, a SEPIC converter was designed by utilizing perturbation and observation (P&O), PSO, and FA, and it was observed that FA minimizes the difficulties of determining global maximum power, reduces convergence, and improves the converter's conversion efficiency [24]. Using the whale optimization technique, a novel approach was proposed in [25] for selecting the PID controller settings of a DC-DC Buck converter. Based on simulation findings, it was discovered that the proposed method was more effective than the genetic algorithm at enhancing the transient response of the Buck converter. The innovative approach for creating fuzzy logic controllers for voltage-regulated DC-DC power converters is suggested in [26]. In order to identify the best feasible membership functions and rules for the fuzzy controller, the multi-objective PSO was utilized to find several pareto-optimal solutions in a multi-objective optimization problem. Furthermore, in [27], the performance of sine-cosine algorithm (SCA) and PSO are compared in coordinating the power of an autonomous hybrid microgrid system with adjustable loads for demand-side management. In [28], the PID controller parameters for a DC-DC Boost converter were tuned using the grey wolf optimizer (GWO) and performances were compared with GA and PSO. The study by the authors of [29] offers a PID controller design using PSO for the best selection of the controller parameters. The outcomes show that the optimization approach is capable of minimizing the aforementioned transient and steady-state faults, which reduce output voltage fluctuations despite input and load side oscillations. The performance and efficiency of the Landsman, SEPIC, and Zeta converters are evaluated in this research [30], where similar investigation was conducted using PSO. However, this study focuses on the following aspects:

(i) Mathematical modeling of a Zeta converter by SSA technique and studying the stability of DC-DC Zeta converter for both open loop and closed-loop case and observing the transient and steady-state responses.

(ii) Studying and implementing swarm intelligent algorithms such as PSO, ACOR, ABC, FA, and SFLA in order to design an optimized PI controller for automated operation for closed-loop case for a Zeta converter reducing the hassle of manual tuning that takes a lot of time and energy.

(iii) Carrying out a detailed comparative analysis in terms of different performance parameters and proposing the most optimized controller for a Zeta converter.

Proper voltage regulation of a Zeta converter is obtained in this paper utilizing a PI controller that has been optimized using several algorithms to determine optimal values for the proportional and integral gains, resulting in improved converter performance. In Section 2, the state space averaging technique is used to model the converter mathematically. The outline of the algorithms is depicted with flowcharts in Section 3, and the algorithm's objective function and SI-based PI controller design are also depicted in this section. The results and simulations, as well as the overall analysis, are presented in Section 4. The MATLAB programming platform is used to run all of the required simulations. Lastly, a comprehensive correlation analysis is provided.

2. State Space Average Method

State space averaging (SSA) is widely employed and a popular method for modeling power converters mathematically. All the derivatives of the circuit have been obtained with the aid of this technique [31]. Piecewise linear networks, where the topology changes at the boundaries between succeeding subintervals within a prototypical switching cycle, are frequently used to describe switched converters. The relevant state-space equations can be determined based on the state of each switching element, such as a transistor or a diode. The energy storage component is usually linked to the state variables [32].

In the Zeta converter (shown in Figure 1), there are two modes of operation. When MOSFET is on the ON-state, the diode is open. So, in this interval, -(V_{in} + V_0) is found across the diode. Also, both the inductors are in the charging phase, which means the current in these inductors is increasing linearly. The capacitor C_1 will be discharged, and energy will be dissipated at the resistor; hence V_0 will increase, and it is connected in series with L_2. The total current of the charging inductor flows through MOSFET.

By Kirchhoff's voltage law (KVL) in Figure 2, the following equations are achieved:

$$\frac{di_{L1}}{dt} = \frac{1}{L_1}\left(-r_{L1}i_{L1} + V_{in}\right),$$

$$\frac{di_{L1}}{dt} = \frac{1}{L_2}\left[-\left(r_{L2} + r_{C1} + \frac{r_{C2}R_O}{r_{C2}+R_O}\right)i_{L2} + V_{C1} - \frac{R_O}{r_{C2}+R_O}V_{C2} + V_{in}\right], \quad (1)$$

$$\frac{dV_{C1}}{dt} = -\frac{i_{L2}}{C_1},$$

$$\frac{dV_{C2}}{dt} = \frac{1}{C_2}\left[\frac{R_O}{r_{C2}+R_O}i_{L2} - \frac{V_{C2}}{r_{C2}+R_O}\right].$$

In the next mode of operation, MOSFET becomes open, and the diode is shorted (Figure 3). Now, both inductors L_1 and L_2 will be discharged. The diode will be forward biased as the voltage polarity of the inductor is changed, and it will conduct.

At this stage, the stored voltage in L_1 and L_2 will be dissipated to capacitor C_1 and the output resistor R_O. As a consequence, both inductor currents decrease linearly. By KVL, we get

$$\frac{di_{L1}}{dt} = -\frac{1}{L_1}\left[-(r_{C2}+r_{L1})i_{L1} - V_{C1}\right],$$

$$\frac{di_{L2}}{dt} = \frac{1}{L_2}\left[-\left(r_{L2} + \frac{r_{C2}R_O}{r_{C2}+R_O}\right)i_{L2} - \frac{R_O}{r_{C2}+R_O}V_{C2}\right]. \quad (2)$$

Current flows through capacitor C_1 with the help of KCL:

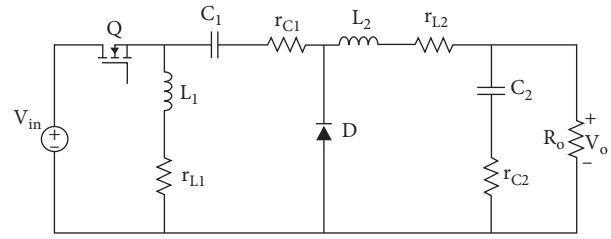

Figure 1: Zeta converter.

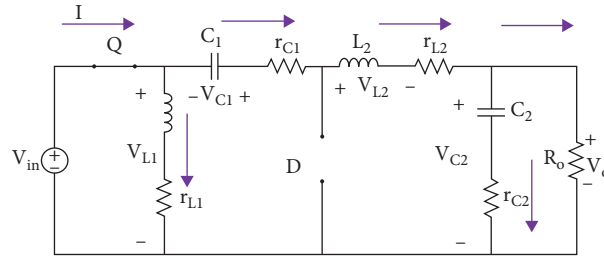

Figure 2: Zeta converter while Q is shorted.

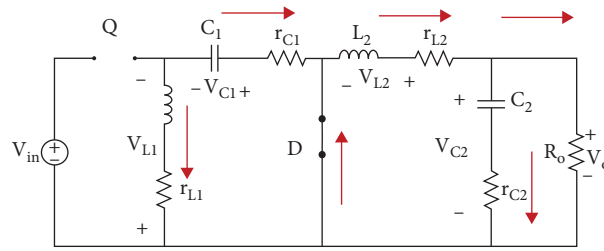

Figure 3: Zeta converter while Q is open.

$$\frac{dV_{C1}}{dt} = -\frac{i_{L1}}{C_1},$$

$$\frac{dV_{C2}}{dt} = \frac{1}{C_2}\left[\frac{R_O}{r_{C2}+R_O}i_2 - \frac{1}{r_{C2}+R_O}V_{C2}\right], \quad (3)$$

$$V_O = \frac{R_O}{r_{C2}+R_O}i_{L2}r_{C2} + \frac{R_O}{r_{C2}+R_O}V_{C2}.$$

The input-output voltage relationship of the Zeta converter is by applying KVL, for inductor L_1 on ON-state and OFF-state, respectively, are $V_{L1} = V_{in}$ and

$$V_{L1} = V_{in}. \quad (4)$$

So, we get

$$V_{C1} = \frac{D}{D-1}V_{in}. \quad (5)$$

Now, the equation for inductor L_2 using KVL is

$$\begin{aligned} &\text{ON state}: V_{L2} = V_{in} - (V_{C1} - V_O), \\ &\text{OFF state}: V_{L2} = -V_O. \end{aligned} \quad (6)$$

Then overall, equation will be

$$V_{C1} = V_{in} - DV_O. \tag{7}$$

Merging, these equations, we get

$$\frac{V_O}{V_{in}} = \frac{D}{1-D}. \tag{8}$$

The SSA equation are obtained using these formulas:

$$\begin{aligned} x'(t) &= Ax(t) + Bu(t), \\ y(t) &= Cx(t) + Bu(t), \end{aligned} \tag{9}$$

where

$$A = A_1 D + A_2 (1-D). \tag{10}$$

And

$$B = B_1 D + B_2 (1-D). \tag{11}$$

Assuming the variables,

$$\begin{aligned} x_1 &= i_{L1}, \\ x_2 &= i_{L2}, \\ x_3 &= V_{C1}, \\ x_4 &= V_{C2}, \\ u(t) &= V_{in}. \end{aligned} \tag{12}$$

State-space equation matrix is given as

$$\begin{bmatrix} X_1 \\ X_2 \\ X_3 \\ X_4 \end{bmatrix} = \begin{bmatrix} -\dfrac{r_{C2}(1-D)+r_{L1}}{L_1} & 0 & \dfrac{1-D}{L_1} & 0 \\ 0 & \dfrac{(r_{C2}+R_O)(Dr_{C1}+r_{L2})+r_{C2}+R_O}{L_2(r_{C2}+R_O)} & \dfrac{D}{L_2} & -\dfrac{R_O}{L_2(r_{C2}+R_O)} \\ \dfrac{1-D}{C_1} & \dfrac{-D}{C_1} & 0 & 0 \\ 0 & \dfrac{R_O}{C_2(r_{C2}+R_O)} & 0 & -\dfrac{1}{C_2(r_{C2}+R_O)} \end{bmatrix} \begin{bmatrix} x_1 \\ x_2 \\ x_3 \\ x_4 \end{bmatrix} + \begin{bmatrix} \dfrac{D}{L_1} \\ \dfrac{D}{L_2} \\ 0 \\ 0 \end{bmatrix} [u(t)]. \tag{13}$$

So,

$$A = \begin{bmatrix} -\dfrac{r_{C2}(1-D)+r_{L1}}{L_1} & 0 & \dfrac{1-D}{L_1} & 0 \\ 0 & \dfrac{(r_{C2}+R_O)(Dr_{C1}+r_{L2})+r_{C2}+R_O}{L_2(r_{C2}+R_O)} & \dfrac{D}{L_2} & -\dfrac{R_O}{L_2(r_{C2}+R_O)} \\ \dfrac{1-D}{C_1} & \dfrac{-D}{C_1} & 0 & 0 \\ 0 & \dfrac{R_O}{C_2(r_{C2}+R_O)} & 0 & -\dfrac{1}{C_2(r_{C2}+R_O)} \end{bmatrix},$$

$$B = \begin{bmatrix} \dfrac{D}{L_1} \\ \dfrac{D}{L_2} \\ 0 \\ 0 \end{bmatrix}, \tag{14}$$

$$C = \begin{bmatrix} 0 & \dfrac{r_{C2}R_O}{r_{C2}+R_O} & 0 & \dfrac{R_O}{r_{C2}+R_O} \end{bmatrix},$$

$$D = [0].$$

System matrix, control matrix, output matrix, and feedforward matrix are represented by A, B, C, and D, respectively. x, u, and y are the state vector, input vector, and output vector, accordingly. A_1 and B_1 also are mentioned for the ON-state. A_2 and B_2 are noted for the OFF-state, correspondingly.

3. Implementation of Swarm Intelligence Algorithms

3.1. Outline of the Algorithms. Swarm intelligence (SI) algorithm refers to a type of optimization technique that is evolving, that is collective intellect of swarms of simple entities [33]. Developing algorithms with swarm intelligence necessitates adaptability to internal and external changes, as well as robustness in the face of individual failures. In the following section, five SI algorithms are studied and implemented for the stability operation of the Zeta converter.

3.1.1. Particle Swarm Optimization (PSO). PSO, proposed by Eberhart and Kennedy in 1995, is a stochastic optimization technique based on swarm that iteratively refines solution candidates. The method is based on sharing information among particle individuals and the particles use their own positions by previous information regarding the best location in the group. It starts with a population of randomly generated solutions, particles with a velocity and a location [34]. The solution particles in this circumstance move through the search region at dynamically balanced velocities as part of a process. The local best-known position of particles and the best-known positions in the search space in iteration $(t-1)$ influence particle movement in iteration t toward optimum solutions are represented as $p\text{best}_s^{t-1}$ and $g\text{best}_s^{t-1}$. Particle i's position and velocity in dimension s of optimization space are represented by (x_{is}^t) and (v_{is}^t), which are written as follows:

$$v_{is}^t = wv_{is}^{t-1} + c_1 b_1^t\left(p\text{best}_{is}^{t-1} - x_{is}^{t-1}\right) + c_2 b_2^t\left(g\text{best}_s^{t-1} - x_{is}^{t-1}\right),$$
$$x_{is}^t = x_{is}^{t-1} + v_{is}^t. \tag{15}$$

3.1.2. Artificial Bee Colony (ABC). ABC is a swarm-based meta-heuristic algorithm developed by Karaboga (2005) for numerical problem optimization. The algorithm is based on Tereshko and Loengarov's (2005) model for honey bee colony foraging behavior [35]. In the solution space, food sources distributed throughout nature are referred to as solutions. The ABC algorithm's conceptualization converts natural processes and activities into algorithmic components and functionalities, where a "food source" is translated into a "feasible solution," and a "nectar amount" is recognized as the fitness of a solution denoted by $F(x_i)$ as provided in the following equation:

$$F(x_i) = \begin{cases} \dfrac{1}{1+f(x_i)}, & f(x_i) \geq 0, \\ 1 + \left|f(x_i)\right|, & \text{otherwise.} \end{cases} \tag{16}$$

Equation (17) calculates the probability of a specific food source being chosen by the ABC algorithm, while (17) generates a neighboring solution such as

$$x_n = x_i + v_i,$$
$$p(x_i) = \frac{F(x_i)}{\sum_{j=1}^{N} F(x_i)}, \tag{17}$$
$$v_i = x_i + \varphi(x_i - x_n),$$

where x_i, x_n, and v_i refer to the current, neighbor, and candidate solutions, respectively, "i" is random number, and N denotes the index of the food source.

$$x_{i,j} = LB_j + r\text{and}(0,1) * \left(UB_j - LB_j\right), \tag{18}$$

where $x_{i,j}$ is the j^{th} decision variable as a member of the x_i solution vector; $j = 1, 2, \ldots, D$ is the index, D is the total number of decision variables, and LB and UB are the decision variable's upper and lower boundary values.

3.1.3. Firefly Algorithm (FA). FA was proposed by Yang created in 2008, which is a revolutionary SI algorithm that imitates the behavior of fireflies in group encounters [36]. To simplify the composition of the FA, Yang et al. included these three rules. First, there is no gender distinction among the firefly. Second, a more visible firefly will attract a less visible one. Third, the brightness of each firefly is determined by the goal function's fitness. The light intensity $I(r)$ varies monotonically and exponentially with the distance r in its simplest form.

$$I = I_0 e^{-\gamma r}, \tag{19}$$

where, I_o represents the initial light intensity and γ represents the light absorption coefficient. According to the abovementioned criteria, each firefly's attraction is proportional to its light intensity; consequently, the attractiveness (beta) is stated as

$$\beta(r) = \beta_0 e^{-\gamma r^2}, \tag{20}$$

where "r" represents the Euclidean distance between two fireflies and "β_o" represents the minimum attractiveness at $r = 0$. The light absorption coefficient is indicated by parameter "γ," which is normally set to 1.

The Euclidean distance "r_{ij}" between two randomly selected fireflies x_i and x_j in the same search space can be determined as

$$r_{i,j} = \left\|X_i - X_j\right\| = \sqrt{\sum_{d=1}^{D}\left(x_{id} - x_{jd}\right)^2}, \tag{21}$$

where "D" is the dimension of the problem.

Any firefly x_i moving towards a brighter firefly x_j is expressed as follows:

$$x_{id}(t+1) = x_{id}(t) + \beta_0 e^{-\gamma r_{ij}^2}\left(x_{jd}(t) - x_{id}(t)\right) + \alpha\varepsilon, \quad (22)$$

where the d_{th} dimension values of firefly "i" and "j," respectively, are X_{jd} and X_{id}. Furthermore, "ε" is a random number with the range [−0.5, 0.5], and "α" is a random value with the range [0, 1]. Finally, the number of iterations is denoted by "t".

3.1.4. Shuffled Frog Leaping Algorithm (SFLA). Eusuff and Lansey presented SFLA in 2003 as an evolutionary optimization strategy based on swarm intelligence that mimics the foraging behavior of frogs for searching global optimum [37]. SFLA refers to a bionic optimization algorithm inspired by frog foraging behavior that fully utilizes the individual generation approach of the memetic algorithm (MA) as well as the information exchange mechanism of the PSO. The technique for splitting the population into memeplexes is as follows: the first frog is assigned to the first memeplex M1, the second to the second memeplex M2, the third to the third memeplex Ms, the fourth to the fourth memeplex Ms, and so on.

3.1.5. Ant Colony Optimization for Continuous Domain (ACOR). Ant colony optimization for continuous domain (ACOR) is a dependable population-based algorithm for solving discrete problems that mimic the foraging behavior of ants [38]. The core idea of ACOR is to switch from a discrete to a continuous probability distribution, i.e., a probability density function (PDF). In ACOR, ant samples refer to PDF. A probability density function can theoretically be any function $P(x)$, such that

$$\int_{-\infty}^{\infty} P(x)\mathrm{d}x = 1. \quad (23)$$

In ACOR, solutions are archived in a file called solution archive. The solution archive is initialized at the start of the process by randomly generating solutions. After all solutions have been collocated, they are reserved, and the rest are discarded. The following is how the mentioned standard deviation should be determined in this direction:

$$\sigma_1^i = \xi \sum_{e=1}^{k} \frac{\left|s_e^i - s_1^i\right|}{k-1},\ I = 1, 2, 3, \ldots\ldots\ldots, n. \quad (24)$$

The positive parameter ξ is constant across all dimensions and has an effect comparable to the ACOR's pheromone evaporation rate.

3.2. Objective Functions. The primary objective is to check the transient behavior of the converter and inspect its stability in the open-loop and closed-loop system. However, the instability can be mitigated by employing a manually tuned PI tuner. But, the process is quite time consuming and a lot of effort has to be invested. For this context, the responsibility of tuning and selecting the most optimized parameters of the controller is handed over to SI algorithms. The analysis is carried out in MATLAB and Simulink.

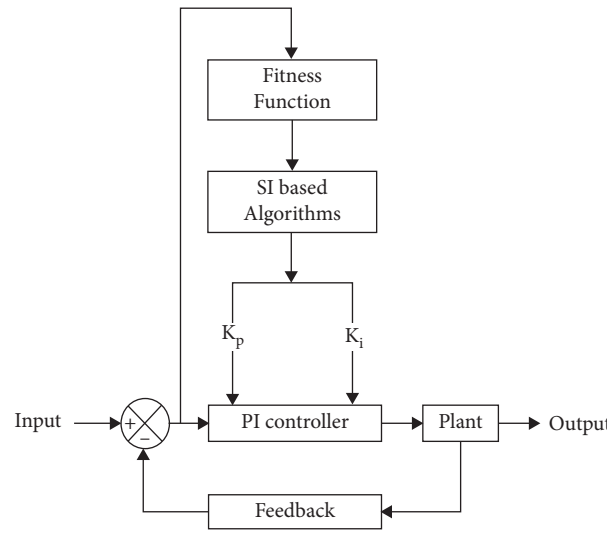

Figure 4: Flowchart of SI-based PI controller [11].

Table 1: Parameters of the Zeta converter.

Parameter	Symbol	Value
Input voltage	V_{in}	20 V
Output voltage	V_o	19.92 V
Duty cycle	D	50%
Switching frequency	F_s	100 KHz
Inductor	L_1	100 μH
	L_2	55 μH
Resistance	r_{L1}	0.001 Ω
	r_{L2}	0.00055 Ω
	r_{C1}	0.19 Ω
	r_{C2}	0.095 Ω
Capacitor	C_1	100 μF
	C_2	200 μF
Load resistance	R	5 Ω

The performance factors of the control instruments are analyzed in the form of error formulas to state the objective functions. The objective functions introduce the performance parameter, which aids in illustrating the stability and effectiveness of the converter. Three error functions are used in this paper. The formulas are as follows:

$$\begin{aligned} IAE &= \int_0^{t_{ss}} |e(t)|\mathrm{d}t, \\ ISE &= \int_0^{t_{ss}} e^2(t)\mathrm{d}t, \\ ITAE &= \int_0^{t_{ss}} t|e(t)|\mathrm{d}t, \\ ITSE &= \int_0^{t_{ss}} te^2(t)\mathrm{d}t. \end{aligned} \quad (25)$$

3.3. Design of the SI-Based PI Controller. Swarm intelligence algorithms are used to find the best values for the proportional integral (PI) controller parameters Kp and Ki. All potential

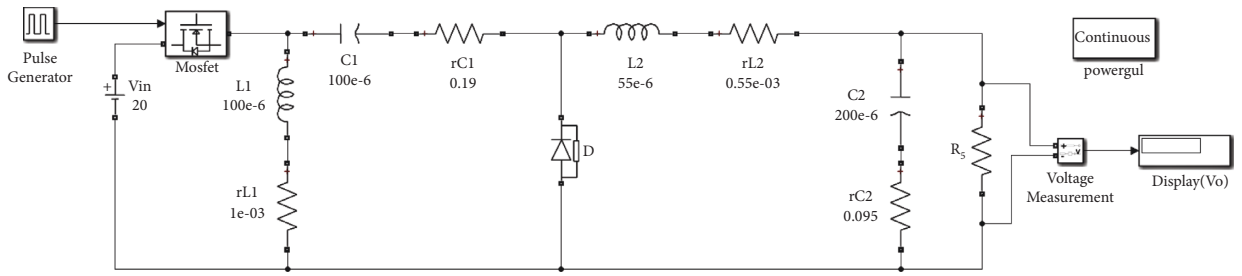

Figure 5: Simulink model of the Zeta converter.

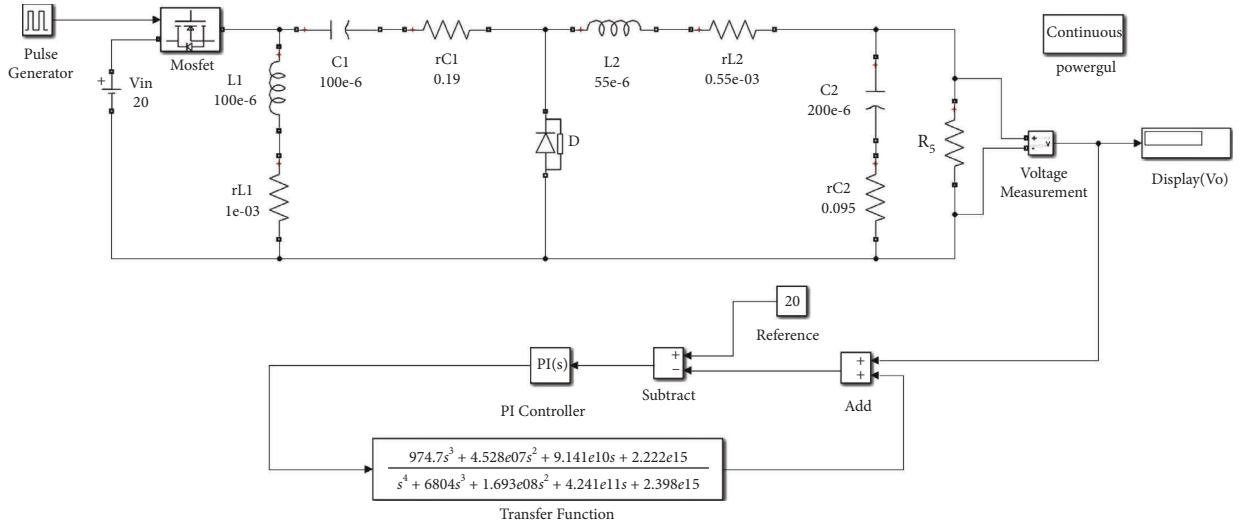

Figure 6: PI-implemented Simulink model of Zeta converter.

sets of controller parameter values are particles with their values changed to minimize the objective function, which in this case is the error criteria. It is ensured that the estimated controller settings result in a reliable closed-loop system for the PI controller architecture. The shape of the closed-loop system transient response to some input signal, such as a step or ramp input, is commonly related to the performance objectives from a control standpoint, as shown in Figure 4.

4. Simulation Results and Stability Analysis

The relevant simulations have been carried out using MATLAB and Simulink to acquire a detailed understanding of the Zeta converter's stability. Therefore, Table 1 contains the recommended parameters for converter [11].

The Zeta converter Simulink model has been built and illustrated in Figure 5, from which the open-loop transfer function of the system has been determined, as shown in the following formula:

$$\frac{974.7s^3 + 4.528 \times 10^7 s^2 + 9.141 \times 10^{10} s + 2.222 \times 10^{15}}{s^4 + 6804s^3 + 1.693 \times 10^8 s^2 + 4.241 \times 10^{11} s + 2.398 \times 10^{15}}. \tag{26}$$

The closed-loop transfer function has been obtained by integrating a PI controller with the open-loop system depicted in Figure 6, which is provided in the following formula:

$$\frac{1.864 \times 10^5 s^4 + 8.663 \times 10^9 s^3 + 1.759 \times 10^{13} s^2 + 4.252 \times 10^{17} s + 4.968 \times 10^{18}}{s^5 + 1.932 \times 10^5 s^4 + 8.833 \times 10^9 s^3 + 1.801 \times 10^{13} s^2 + 4.276 \times 10^{17} s + 4.968 \times 10^{18}}. \tag{27}$$

Hence, the step response of the closed-loop system has been examined, revealing a 10.5% overshoot as shown in Figure 7. The output of the conventional PI controlled Zeta converter has been shown in Table 2. For each of the

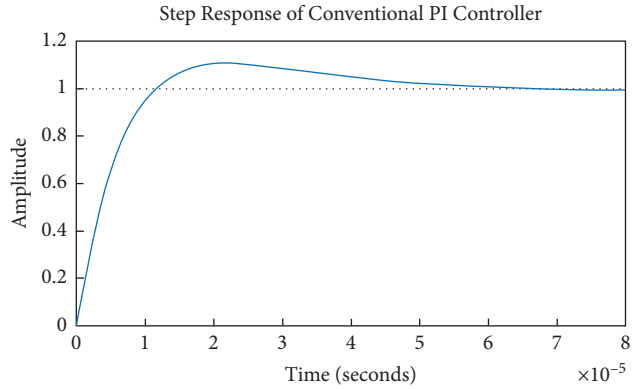

Figure 7: Step response of the conventional PI controller.

Table 2: Output of the conventional PI-based Zeta converter.

Attributes	Symbols	Values
Gain values	Kp	191.2786
	Ki	2236.0087
Performance parameters	%OS	10.4559
	Tr (seconds)	$8.2167e-06$
	Ts (seconds)	$4.9872e-05$
	Peak amplitude	1.1046

Table 3: Parameters of ABC.

Parameters	Values
Acceleration coefficient upper bound	0.02
Abandonment limit parameter (trial limit)	24
Number of onlooker bees	20
Population size	20
No of iterations	50

Table 4: Parameters of ACOR.

Parameters	Values
Deviation-distance ratio	0.015
Intensification factor (selection pressure)	0.05
Sample size	10
Population size	20
No of iterations	50

Table 5: Parameters of PSO.

Parameters	Values
Personal acceleration coefficient	0.002
Social acceleration coefficient	0.004
Damping ratio of inertia coefficient	0.099
Inertia coefficient	1.5
Population size	20

Table 6: Parameters of FA.

Parameters	Values
Mutation coefficient damping ratio	1.8
Mutation coefficient	0.051293
Attraction coefficient base value	0.08293
Light absorption coefficient	0.06439
Population size	20

Table 7: Parameters of SFLA.

Parameters	Values
Number of iterations within each memeplex	2
Step size	1.1
Number of offspring	4
Number of memeplexes	2
Memeplex size	10

algorithm, 20–30 iterations have been performed and the related data have been gathered. To compare the algorithms, their average value has been utilized.

4.1. Step Response Analysis. All the parameters of ABC, ACOR, PSO, FA, and SFLA algorithms have been tabulated in Table 3, Table 4, Table 5, Table 6, and Table 7, respectively. However, the corresponding fitness functions (IAE, ITAE, ISE, and ITSE), and the relevant responses have been recorded in Table 8, Table 9, Table 10, Table 11, and Table 12, consecutively. Hence, the comparative analysis among the controllers has been presented in Figures 8–12, respectively.

4.2. Eigenvalue Analysis. The proposed algorithms' capacity to achieve system stability is determined using eigenvalue analysis. The analysis is performed by using four specified objective functions consist of IAE, ITAE, ISE, and ITSE. The real portion of the eigenvalue offers information about the system's stability. The system is said to be stable when the real component of the eigenvalue lies on the left side of the "s" plane [39]. Table 13 demonstrates the eigenvalues for each objective function of five swarm-based algorithms. Four Eigenvalues are obtained for each objective function, including two complex values, as stated in the table. However, from Figure 13 to Figure 17, it is visually evident that their imaginary parts are placed in such a way that they appear to cancel each other out apparently. Furthermore, the

Table 8: Output of the ABC-PI-based Zeta converter.

Attributes	Symbols	ABC-PI			
		IAE	ITAE	ISE	ITSE
Gain values	Kp	909.6358	1236.8	1059.4	1347
	Ki	573.889	883.2359	737.454	1010.5
Performance parameters	%OS	3.4288	2.6524	3.0223	2.4658
	Tr (seconds)	$2.2123e-06$	$1.6707e-06$	$1.9261e-06$	$1.5436e-06$
	Ts (seconds)	$1.8665e-05$	$1.2165e-05$	$1.5454e-05$	$1.0340e-05$
	Peak amplitude	1.0343	1.0265	1.0302	1.0247

Table 9: Output of the ACOR-PI-based Zeta converter.

Attributes	Symbols	ACOR-PI			
		IAE	ITAE	ISE	ITSE
Gain values	Kp	1045.5	913.12	1498.3	1261.9
	Ki	1947.8	1989.8	1912	1874.5
Performance parameters	%OS	3.05	3.42	2.25	2.61
	Tr (seconds)	$1.95e-06$	$2.20e-06$	$1.40e-06$	$1.64e-06$
	Ts (seconds)	$1.57e-05$	$1.86e-05$	$8.05e-06$	$1.17e-05$
	Peak amplitude	1.0306	1.0342	1.0225	1.03

Table 10: Output of the PSO-PI-based Zeta converter.

Attributes	Symbols	PSO-PI			
		IAE	ITAE	ISE	ITSE
Gain values	Kp	1433.9	1029.3	1087.6	922.17
	Ki	1479	823.8417	1354.1	1057.6
Performance parameters	%OS	2.3367	3.0959	2.9566	3.3905
	Tr (seconds)	$1.4564e-06$	$1.9775e-06$	$1.8803e-06$	$2.1850e-06$
	Ts (seconds)	$8.9968e-06$	$1.6064e-05$	$1.4898e-05$	$1.8378e-05$
	Peak amplitude	1.0234	1.0310	1.0296	1.0339

Table 11: Output of the FA-PI-based Zeta converter.

Attributes	Symbols	FA-PI			
		IAE	ITAE	ISE	ITSE
Gain values	Kp	907.5887	1032.6	1456.3	1163.8
	Ki	515.012	1577.7	1833.6	1728.9
Performance parameters	%OS	3.4351	3.0877	2.3056	2.7928
	Tr (seconds)	$2.2168e-06$	$1.9717e-06$	$1.4355e-06$	$1.7669e-06$
	Ts (seconds)	$1.8712e-05$	$1.5996e-05$	$8.6626e-06$	$1.3461e-05$
	Peak amplitude	1.0344	1.0309	1.0231	1.0279

Table 12: Output of the SFLA-PI-based Zeta converter.

Attributes	Symbols	FA-PI			
		IAE	ITAE	ISE	ITSE
Gain values	Kp	1107.1	901.8246	1478.9	1007.1
	Ki	1950.1	1874.2	1715.8	1948.7
Performance parameters	%OS	2.9129	3.4532	2.2750	3.1526
	Tr (seconds)	$1.8498e-06$	$2.2296e-06$	$1.4150e-06$	$2.0171e-06$
	Ts (seconds)	$1.4522e-05$	$1.8846e-05$	$8.3296e-06$	$1.6524e-05$
	Peak amplitude	1.0291	1.0345	1.0228	1.0315

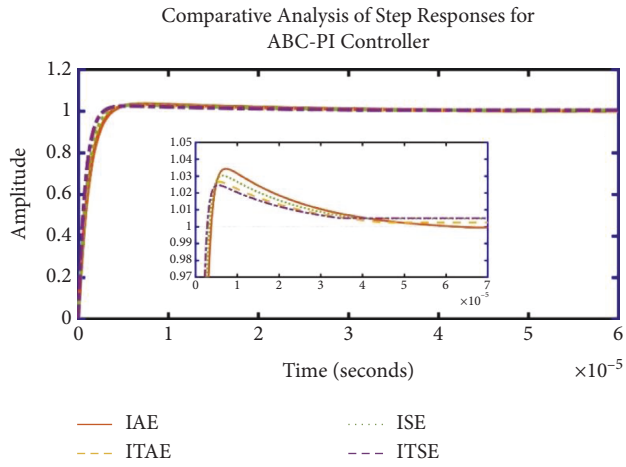

Figure 8: Comparative analysis of step responses for the ABC-PI controller.

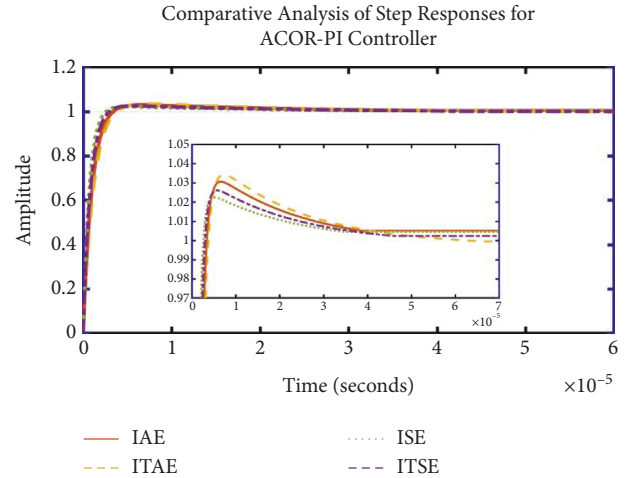

Figure 9: Comparative analysis of step responses for the ACOR-PI controller.

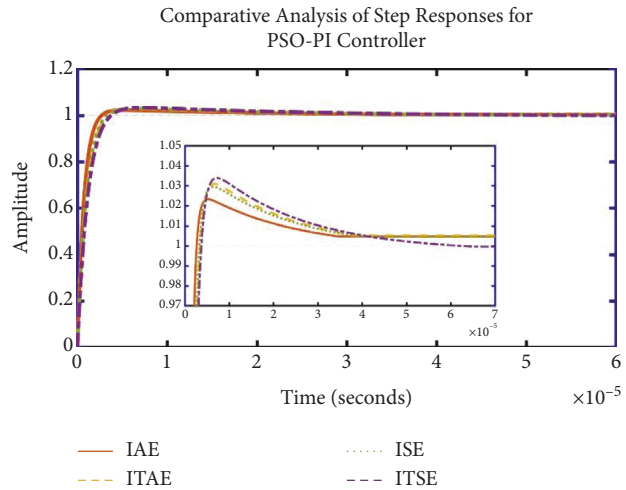

Figure 10: Comparative analysis of step responses for the PSO-PI controller.

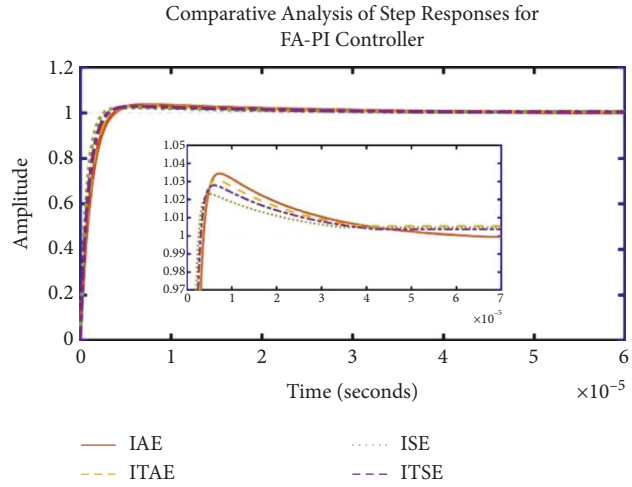

Figure 11: Comparative analysis of step responses for the FA-PI controller.

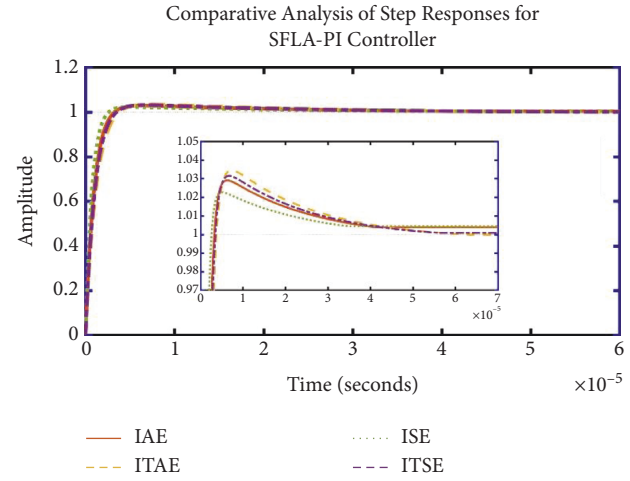

Figure 12: Comparative analysis of step responses for the SFLA-PI controller.

real component of the eigenvalues from five SI-based PI controllers stays on the left side of the "*s*" plane, indicating that the system is stable, as shown in the tables. There is some overlapping of points due to the extensive range of eigenvalues in the figures. As a result, each algorithm's figure is accompanied by four additional figures that represent overlapping spots in a more obvious manner.

4.3. Comparative Analysis. Compared to four fitness functions, for ACOR-PI, FA-PI, and SFLA-PI, the ISE fitness function delivers a lower percentage of overshoot, shorter settling time, lower rise time, and lower peak amplitude. For the ABC-PI and PSO-PI controllers, the ITSE and IAE fitness functions independently yield a lower percentage of overshoot, shorter settling time, lower rising time, and lower peak amplitude when compared to other fitness functions. Furthermore, the stability of the SI-based PI controller is exhibited in figures of eigenvalues. It is evident from the eigenvalue figures that ISE objective function for ACOR-PI is more stable compared to the rest, as it is on the leftmost side of the s-plane, exhibiting the largest negative real part of eigenvalue among all five algorithms. Despite the fact that the ISE objective function for SFLA-PI illustrates remarkably similar stability and step response to ACOR-PI, the peak amplitudes for all fitness functions for each algorithm are almost identical. When comparing these five algorithms, it is apparent that the ACOR-PI controller's ISE fitness function delivers the best response. The top-performing fitness function from each algorithm is presented in Table 14, along with their associated performance parameters.

Overall comparison of percentage of overshoot, rise time, and settling time among the best performing ones are depicted in Figure 18, Figure 19, and Figure 20, respectively. Moreover, in the study [11], the Zeta converter's optimization was carried out using a PID controller that incorporated the particle swarm optimization algorithm.

Table 13: Eigenvalue analysis.

Algorithm	Objective function	Eigenvalues of the system				
			Overlapping points			
			a	b	c	d
PSO	IAE	$1.0e+06*(-1.3565+0i)$	$1.0e+06*(-0.0005+0.0071i)$	$1.0e+06*(-0.0470+0i)$	$-1.025+0i$	$1.0e+06*(-0.0005–0.0071i)$
	ITAE	$1.0e+05*(-9.6151+0i)$	$1.0e+05*(-0.0048+0.0706i)$	$1.0e+05*(-0.4759+0i)$	$-0.8+0i$	$1.0e+05*(-0.0048–0.0706i)$
	ISE	$1.0e+06*(-1.0185+0i)$	$1.0e+06*(-0.0005+0.0071i)$	$1.0e+06*(-0.0475+0i)$	$-1.24+0i$	$1.0e+06*(-0.0005–0.0071i)$
	ITSE	$1.0e+05*(-8.5682+0i)$	$1.0e+05*(-0.0048+0.0706i)$	$1.0e+05*(-0.4786+0i)$	$-1.15+0i$	$1.0e+05*(-0.0048–0.0706i)$
ABC	IAE	$1.0e+05*(-8.4457+0i)$	$1.0e+05*(-0.0048+0.0706i)$	$1.0e+05*(-0.4789+0i)$	$-0.63+0i$	$1.0e+05*(-0.0048–0.0706i)$
	ITAE	$1.0e+06*(-1.1641+0i)$	$1.0e+06*(-0.0005+0.0071i)$	$1.0e+06*(-0.0472+0i)$	$-0.71+0i$	$1.0e+06*(-0.0005–0.0071i)$
	ISE	$1.0e+05*(-9.9092+0i)$	$1.0e+05*(-0.0048+0.0706i)$	$1.0e+05*(-0.4752+0i)$	$-0.698+0i$	$1.0e+05*(-0.0048–0.0706i)$
	ITSE	$1.0e+06*(-1.2717+0i)$	$1.0e+06*(-0.0005+0.0071i)$	$1.0e+06*(-0.0471+0i)$	$-0.75+0i$	$1.0e+06*(-0.0005–0.0071i)$
ACOR	IAE	$1.0e+05*(-9.7734+0i)$	$1.0e+05*(-0.0048+0.0706i)$	$1.0e+05*(-0.4755+0i)$	$-1.88+0i$	$1.0e+05*(-0.0048–0.0706i)$
	ITAE	$1.0e+05*(-8.4797+0i)$	$1.0e+05*(-0.0048+0.0706i)$	$1.0e+05*(-0.4788+0i)$	$-2.19+0i$	$1.0ev+05*(-0.0048–0.0706i)$
	ISE	$1.0e+06*(-1.4193+0i)$	$1.0e+06*(-0.0005+0.0071i)$	$1.0e+06*(-0.0469+0i)$	$-1.28+0i$	$1.0e+06*(-0.0005–0.0071i)$
	ITSE	$1.0e+06*(-1.1886+0i)$	$1.0e+06*(-0.0005+0.0071i)$	$1.0e+06*(-0.0472+0i)$	$-1.5+0i$	$1.0e+06*(-0.0005–0.0071i)$
FA	IAE	$1.0e+05*(-8.4257+0i)$	$1.0e+05*(-0.0048+0.0706i)$	$1.0e+05*(-0.4790+0i)$	$-0.55+0i$	$1.0e+05*(-0.0048–0.0706i)$
	ITAE	$1.0e+05*(-9.6474+0i)$	$1.0e+05*(-0.0048+0.0706i)$	$1.0e+05*(-0.4758+0i)$	$-1.57+0i$	$1.0e+05*(-0.0048–0.0706i)$
	ISE	$1.0e+06*(-1.3784+0i)$	$1.0e+06*(-0.0005+0.0071i)$	$1.0e+06*(-0.0469+0i)$	$-1.26+0i$	$1.0e+06*(-0.0005–0.0071i)$
	ITSE	$1.0e+06*(-1.0929+0i)$	$1.0e+06*(-0.0005+0.0071i)$	$1.0e+06*(-0.0473+0i)$	$-1.5+0i$	$1.0e+06*(-0.0005–0.0071i)$
SFLA	IAE	$1.0e+06*(-1.0375+0i)$	$1.0e+06*(-0.0005+0.0071i)$	$1.0e+06*(-0.0474+0i)$	$-1.786+0i$	$1.0e+06*(-0.0005–0.0071i)$
	ITAE	$1.0e+05*(-8.3693+0i)$	$1.0e+05*(-0.0048+0.0706i)$	$1.0e+05*(-0.4792+0i)$	$-2.09+0i$	$1.0e+05*(-0.0048–0.0706i)$
	ISE	$1.0e+06*(-1.4004+0i)$	$1.0e+06*(-0.0005+0.0071i)$	$1.0e+06*(-0.0469+0i)$	$-1.18+0i$	$1.0e+06*(-0.0005–0.0071i)$
	ITSE	$1.0e+05*(-9.3982+0i)$	$1.0e+05*(-0.0048+0.0706i)$	$1.0e+05*(-0.4764+0i)$	$-1.93+0i$	$1.0e+05*(-0.0048–0.0706i)$

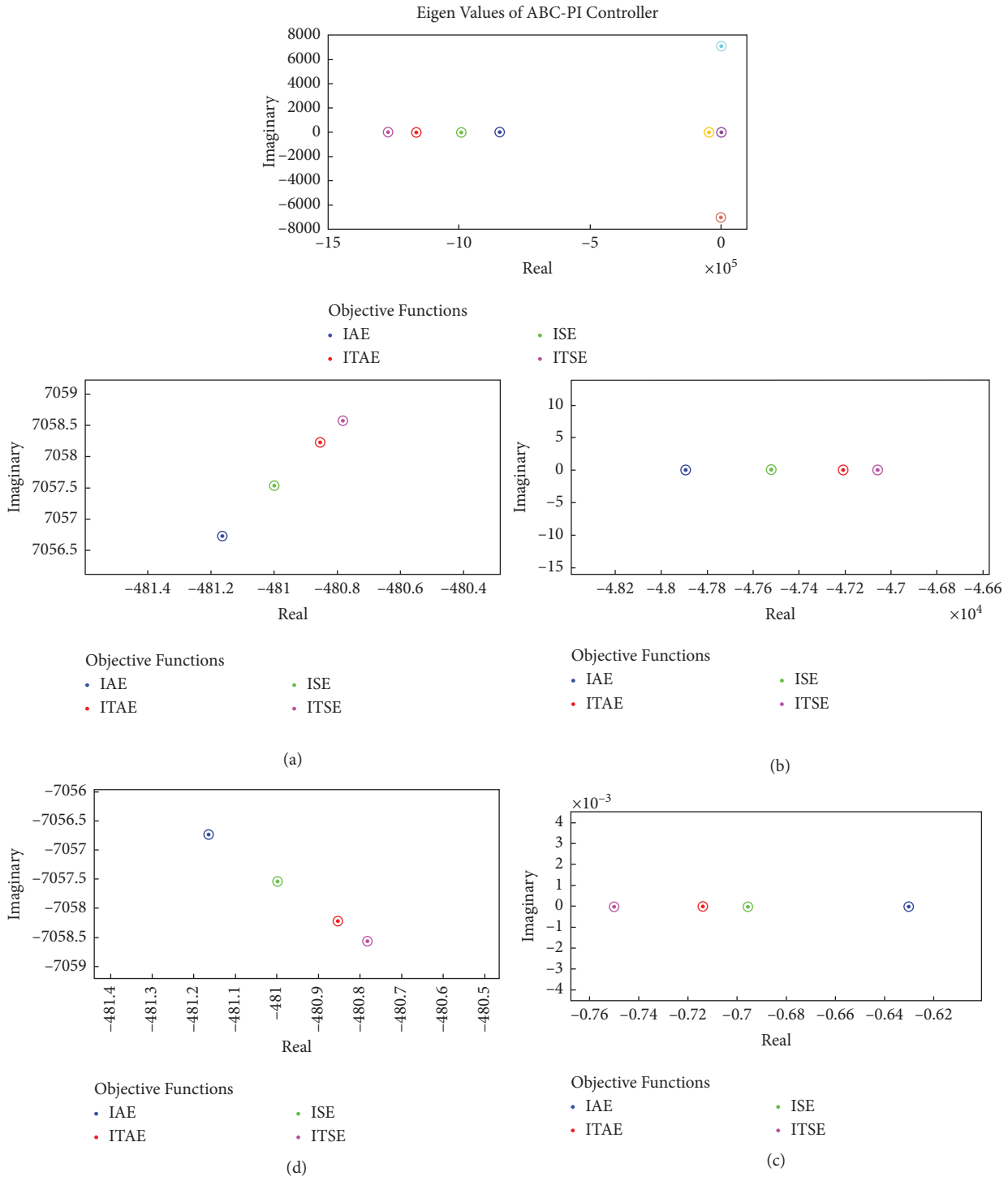

Figure 13: Eigenvalues of the ABC-PI controller.

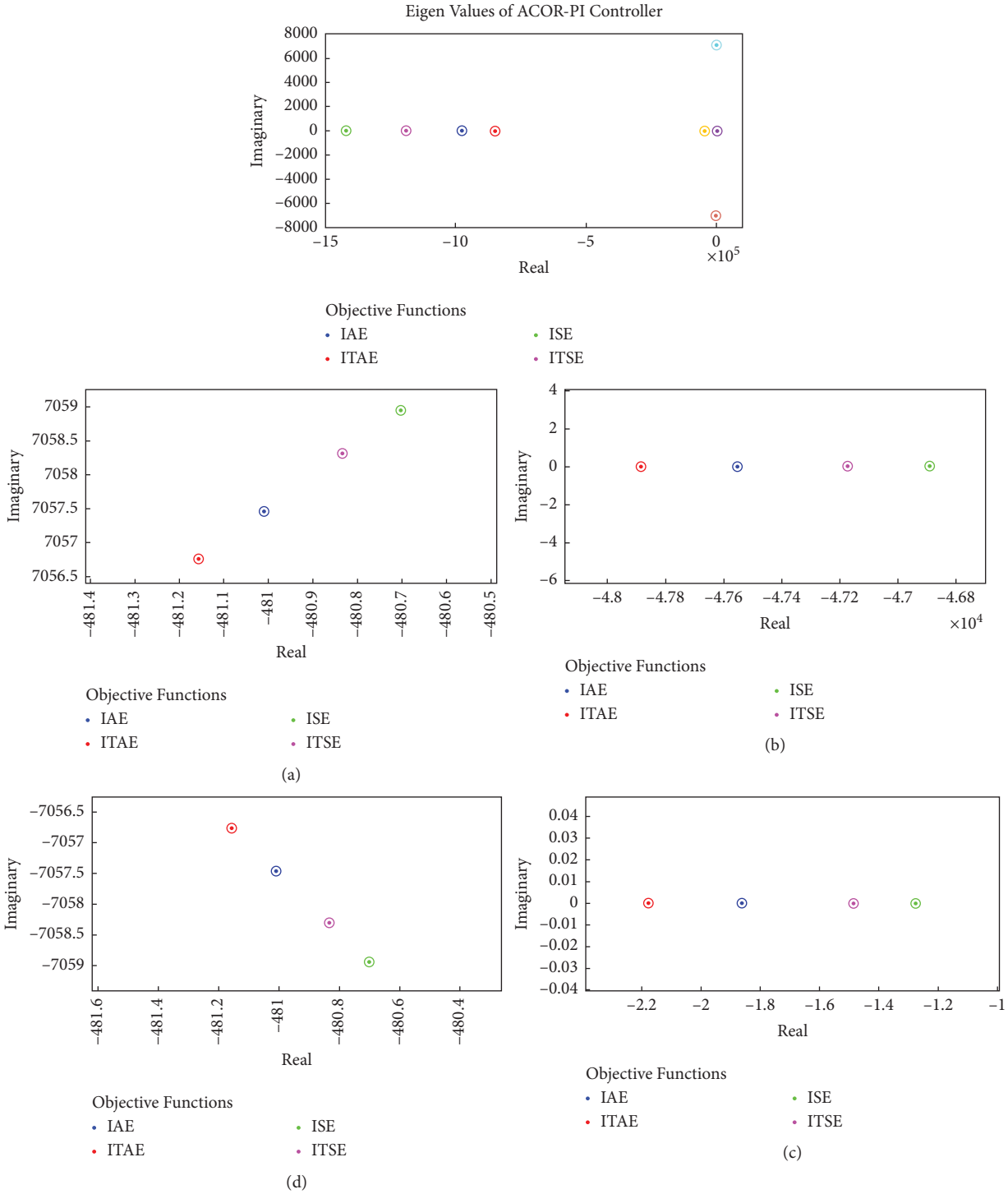

Figure 14: Eigenvalues of the ACOR-PI controller.

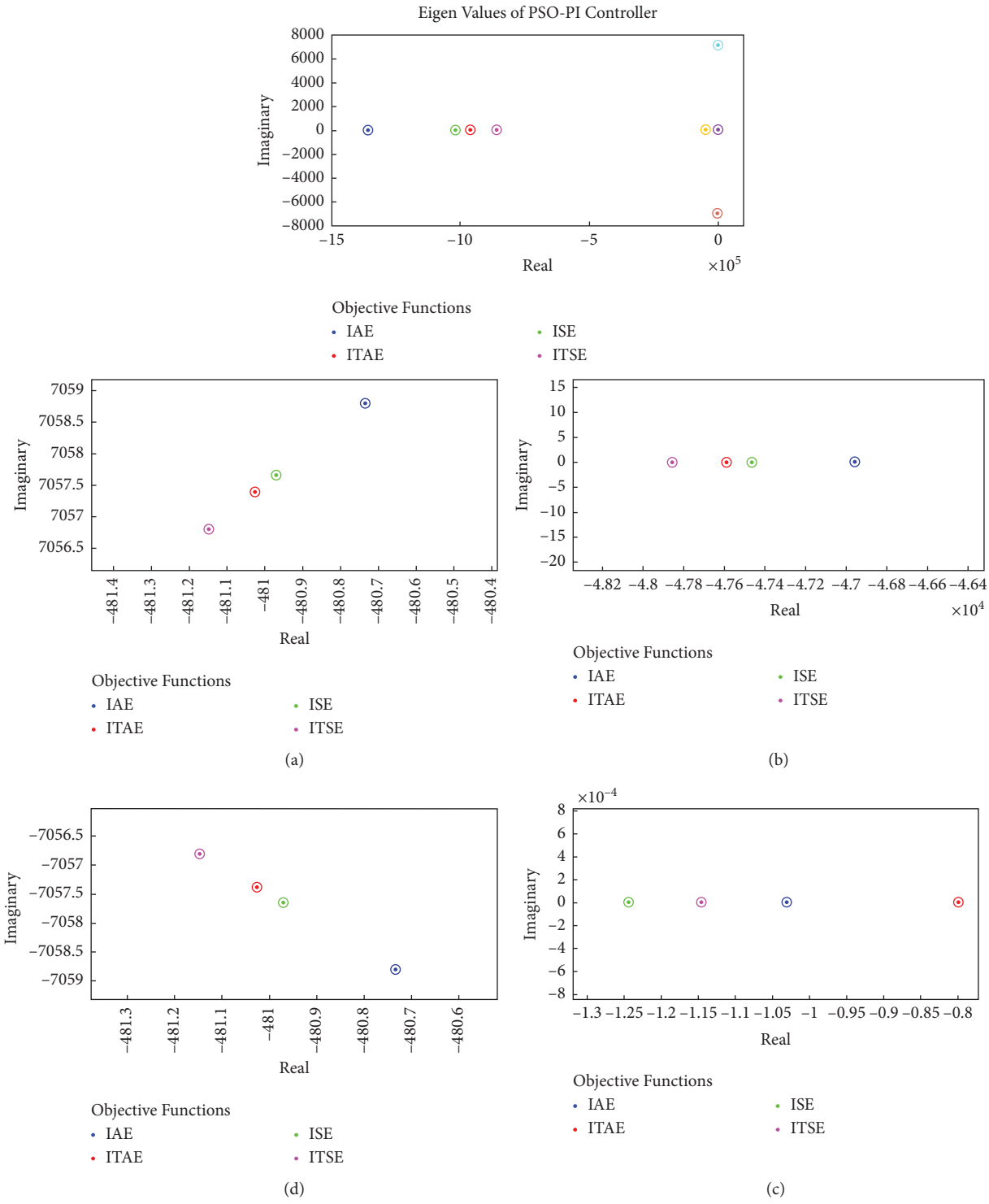

Figure 15: Eigenvalues of the PSO-PI controller.

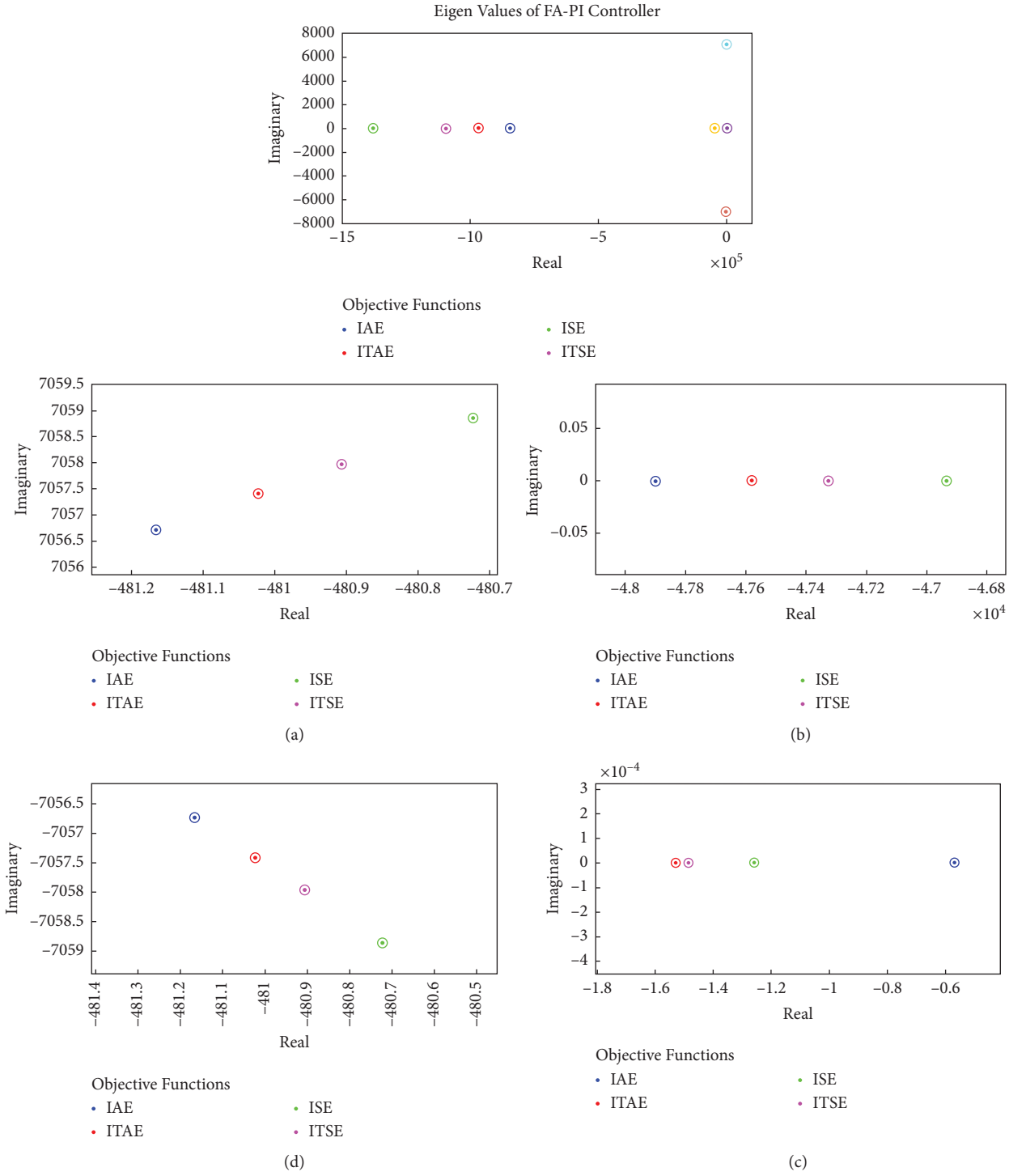

Figure 16: Eigenvalues of the FA-PI controller.

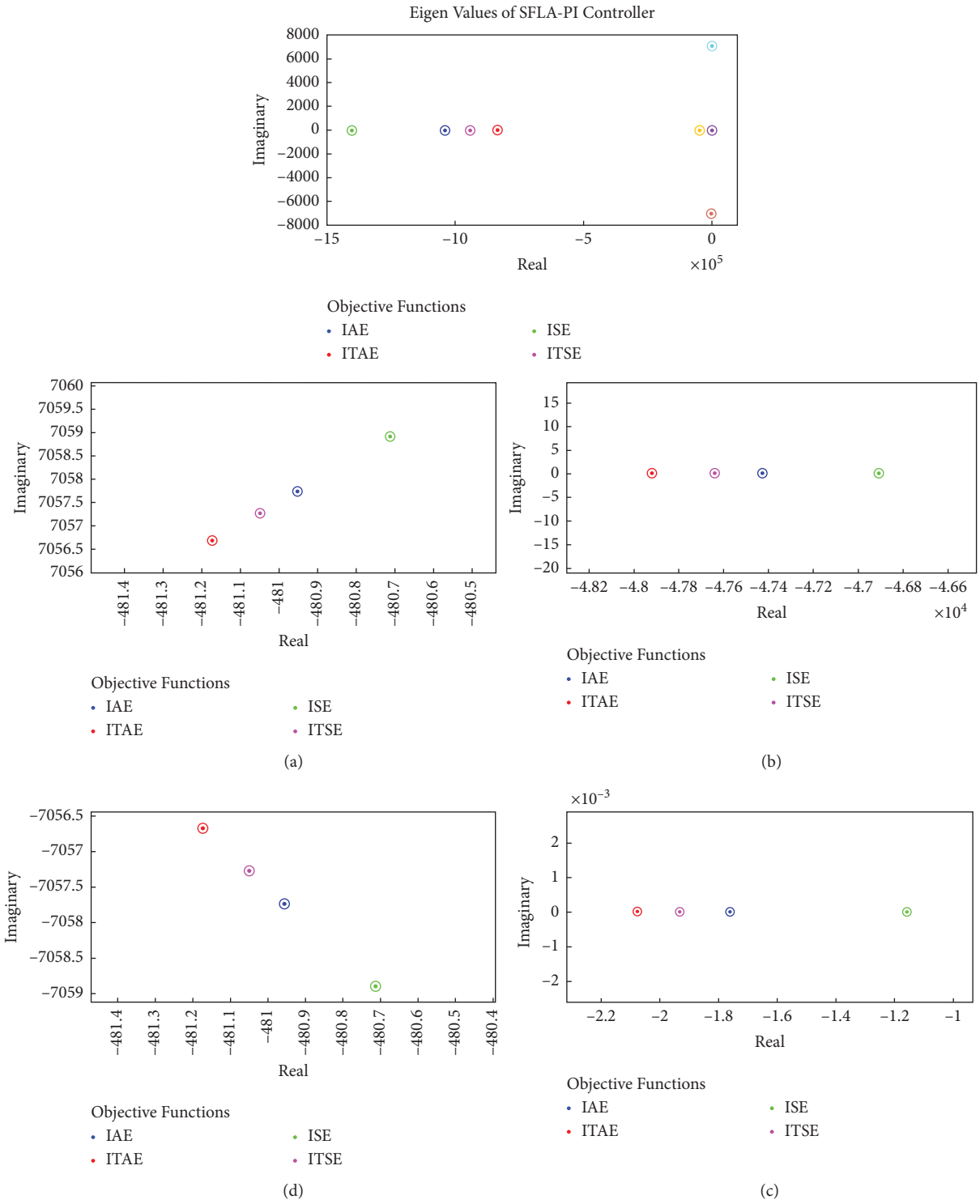

Figure 17: Eigenvalues of the SFLA-PI controller.

However, in this case we used the PI controller which collaborated separately with five swarm intelligence algorithms to perform a comparative analysis. Since the derivative values in our work were so negligible and made no contribution to the optimization, we decided to omit the derivative controller and instead developed a PI controller. Some of the corresponding literature are studied and their outputs are shown in Table 15.

Table 14: Comparative analysis among the SI-based PI controller for the Zeta converter.

Attributes	Controllers				
	ABC-PI	ACOR-PI	PSO-PI	FA-PI	SFLA-PI
Best performing fitness function	ITSE	ISE	IAE	ISE	ISE
Percentage of overshoot (%OS)	2.4658	2.2495	2.3367	2.3056	2.2750
Rise time, tr (seconds)	$1.5436e-06$	$1.3979e-06$	$1.4564e-06$	$1.4355e-06$	$1.4150e-06$
Settling time, ts (seconds)	$1.0340e-05$	$8.0472e-06$	$8.9968e-06$	$8.6626e-06$	$8.3296e-06$
Peak amplitude	1.0247	1.0225	1.0234	1.0231	1.0228

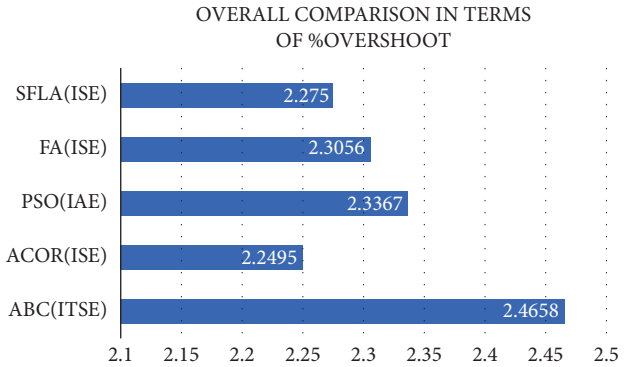

Figure 18: Overall comparison in terms of %Overshoot.

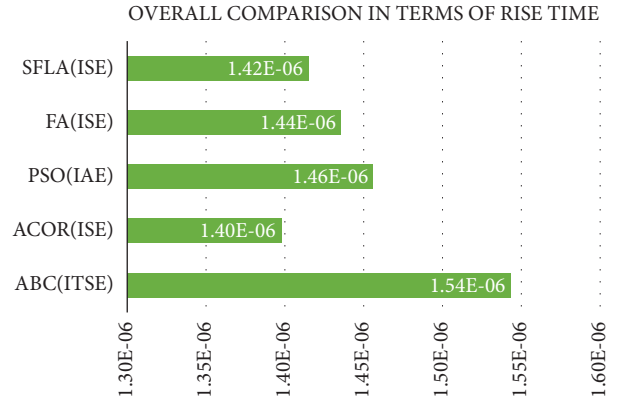

Figure 19: Overall comparison in terms of rise time.

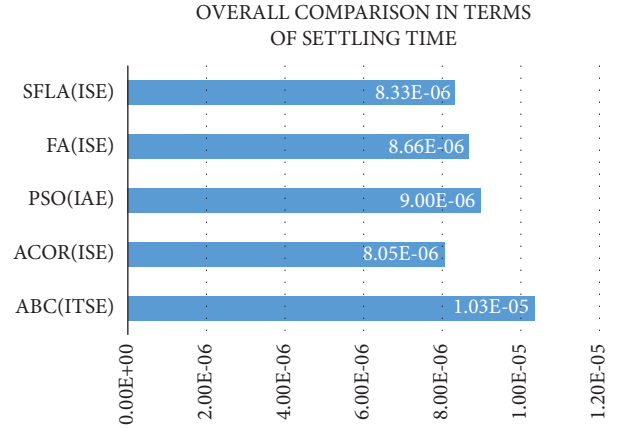

Figure 20: Overall comparison in terms of settling time.

Table 15: Output of different literature studies.

Ref	Converter	Controller	Algorithm	Function	%OS	Year
[40]	Buck	FOPID	CI	ISE ITSE	5.6 9.2	2021
[41]	Buck	PID	GA	IAE	4.17	2020
[42]	Boost	FOFPID	MFO PSO	ISE, IAE ISE, IAE	3.14 3.13	2020
[43]	Buck	PID	FA	MSE ITSE	11.118 10.6834	2014
[44]	SEPIC	DFOPID	QPSO	ITAE	7.3	2020
[45]	Boost Interleaved boost	Optimal type 3	PSO	ITAE	6.67 3.33	2016
[46]	Boost	PID	GSA	ITAE	3.31	2016
[47]	Buck	PI	PSO	IAE	6.04	2020
Proposed work	Zeta	PI	ACOR	ISE	2.2495	2022

5. Conclusion

After observing all the simulation results, it is evident that the ACOR-PI controller outperforms the other controllers in terms of percentage of overshoot (2.27%), rise time (1.54 μs), and settling time (0.103 μs). In addition, it is worth mentioning that both the PSO-PI and ABC-PI controllers provid effective responses. Furthermore, among the four objective functions (IAE, ITAE, ISE, and ITSE), the ISE objective function offered remarkable responses for three swarmed-based PI controller (ACOR-PI, SFLA-PI, and FA-PI). For the other two, IAE for PSO-PI and ITSE for ABC-PI yielded better responses. Hence, applying eigenvalue analysis, it is observed that the real parts of eigenvalues from five swarmed-based PI controllers are negative, indicating that the system is stable for all five PI controllers. The eigenvalue figures are also depicting that the ISE objective function for ACOR-PI is providing the largest negative real value compared to all five swarmed-based PI controllers, revealing that the system is more stable for this controller. However, there is not much of a performance difference between them, especially with ACOR-PI and SFLA-PI controllers and so, it can be concluded that both controllers will be best suited for Zeta converter. In the future, we plan to use a modeling technique based on machine learning to synthesize the response of power converters which will enable us to develop an alternative design methodology for power electronic devices that relies on artificial intelligence (AI) techniques rather than conventional approaches.

Abbreviations

SI: Swarm intelligence
SSA: State space averaging
PI: Proportional integral
IAE: Integral absolute error
ITAE: Integral time absolute error
ISE: Integral square error
ITSE: Integral time square error
EV: Electrical vehicle
MPPT: Maximum power point
K_p: Proportional gain
K_i: Integral gain
PSO: Particle swarm optimization
ACO: Ant colony optimization
ACOR: Ant colony optimization for continuous domain
ABC: Artificial bee colony
FA: Firefly algorithm
SFLA: Shuffled frog leaping algorithm
GSA: Gravitational search algorithm
SMC: Sliding mode control
GA: Genetic algorithm
P&O: Perturb and observe
V_{in}: Input voltage
V_o: Output voltage
C_1, C_2: Capacitors
L_1, L_2: Inductors
r_{L1}, r_{L2}: Stray resistance of inductors
i_{L1}, i_{L2}: Inductor current
(di_{L1}/dt), (di_{L2}/dt): Change of inductor current through an inductor
r_{C1}, r_{C2}: Stary resistance of capacitors
R_o: Load resistance
V_{C1}, V_{C2}: Capacitor voltage
V_{L1}, V_{L2}: Inductor voltage
(dV_{C1}/dt), (dV_{C2}/dt): Change in capacitor voltage
D: Duty cycle
x: State vector
y: Output vector
u: Input vector
A: System matrix
B: Control matrix
C: Output matrix
D: Feed forward matrix
x_{is}^t: Optimized position of i's particle
v_{is}^t: Velocity of i's particle
c_1, c_2: Acceleration coefficient
w: Inertia weight

b_1, b_2: Boundaries
$p\text{best}_s^{t-1}$: Best known position locally
$g\text{best}_s^{t-1}$: Best position in search space
x_n: Neighbor
x_i: Current solution
v_i: Candidate solution
I: Intensity of light
γ: Light absorption coefficient
β: Function of attractiveness
r: Euclidean distance
X_i, X_j: Butterflies
D: Dimension of the problem
α, ε: Random number
MA: Memetic algorithm
OS: Overshoot
T_r: Rising time
T_s: Settling time.

Data Availability

The data used to support the findings of this study are available within this article.

Conflicts of Interest

The authors declare that there are no conflicts of interest.

References

[1] M. Bhuyan, D. C. Das, A. K. Barik, and S. C. Sahoo, "Performance assessment of novel solar thermal-based dual hybrid microgrid system using CBOA optimized cascaded PI-tid controller," *IETE Journal of Research*, pp. 1–18, 2022.

[2] S. Peyghami, T. Dragicevic, and F. Blaabjerg, "Intelligent long-term performance analysis in power electronics systems," *Scientific Reports*, vol. 11, pp. 1–18, 2021.

[3] A. Almutairi, K. Sayed, N. Albagami, A. G. Abo-Khalil, and H. Saleeb, "Multi-port PWM DC-DC power converter for renewable energy applications," *Energies*, vol. 14, p. 3490, 2021.

[4] M. M. Nishat, F. Faisal, M. A. M. Oninda, and M. A. Hoque, "Modeling, simulation and performance analysis of SEPIC converter using hysteresis current control and PI control method," in *Proceedings of the 2018 Int. Conf. on Inv. in Science, Engg. and Tech. (ICISET)*, pp. 7–12, Chittagong, Bangladesh, October 2018.

[5] M. M. Nishat, F. Faisal, and M. A. Hoque, "Modeling and stability analysis of a DC-DC SEPIC converter by employing optimized PID controller using genetic Algorithm," *International Journal of Electrical & Computer Sciences IJECS-IJENS*, vol. 19, no. 1, pp. 1–7, 2019.

[6] M. M. Nishat, F. Faisal, M. Rahman, and M. A. Hoque, "Modeling and design of a fuzzy logic based PID controller for DC motor speed control in different loading condition for enhanced performance," in *Proceedings of the 2019 1st Int. Conference on Advances in Science, Engg. And Robotics Tech. (ICASERT)*, pp. 1–6, IEEE, Dhaka, Bangladesh, May 2019.

[7] M. M. Nishat, "Stability analysis and optimization of simulated annealing (SA) algorithm based PID controller for DC-DC SEPIC converter," *International Journal of Computer Network and Information Security*, vol. 19, no. 9, pp. 1–8.

[8] M. B. Rashid, M. A. M. Oninda, F. Faisal, M. M. Nishat, G. Sarowar, and M. A. Hoque, "A novel topology of single-phase AC-DC integrated boost-SEPIC (IBS) converter using common Part Sharing method (CPSM) for high step-up applications," *JPEE*, vol. 6, no. 6, pp. 38–47, 2018.

[9] M. D. Rahman, F. Faisal, M. M. Nishat, and M. R. K. Shagor, "Design and Analysis of Passive LC^3Component Boost Converter," in *Proceedings of the 2021 IEEE Madras Section Conference (MASCON)*, pp. 1–6, Chennai, India, January2021.

[10] S. Oommen, B. Adithya, A. Burri, and M. H. Ananda, "Zeta converter simulation for continuous current mode operation," *International Journal of Advanced Research in Engineering & Technology*, vol. 10, 2019.

[11] M. M. Nishat, M. R. K. Shagor, H. Akter, S. A. Mim, and F. Faisal, "An optimal design of PID controller for DC-DC zeta converter using particle swarm optimization," in *Proceedings of the 23rd International Conference on Computer and Information Technology (ICCIT)*, December 2010.

[12] W. Sun, M. Tang, L. Zhang, Z. Huo, and L. Shu, "A survey of using swarm intelligence algorithms in IoT," *Sensors*, vol. 20, p. 1420, 2020.

[13] D. Wang, D. Tan, and L. Liu, "Particle swarm optimization algorithm: an overview," *Soft Computing*, vol. 22, pp. 387–408, 2018.

[14] D. Karaboga, "Artificial bee colony algorithm," *Scholarpedia*, vol. 5, p. 6915, 2010.

[15] M. R. K. Shagor, A. J. Mahmud, M. M. Nishat, F. Faisal, M. H. Mithun, and M. A. Khan, "Firefly algorithm based optimized PID controller for stability analysis of DC-DC SEPIC converter," in *Proceedings of the 12th Annual Ubiquitous Comp., Elec. & Mobile Comm. Conf. (UEMCON)*, pp. 0957–0963, New York, NY, USA, December 2021.

[16] M. L. Pérez-Delgado, "Color image quantization using the shuffled-frog leaping algorithm," *Engineering Applications of Artificial Intelligence*, vol. 79, pp. 142–158, 2019.

[17] M. Dorigo and T. Stützle, "Ant colony optimization: overview and recent advances," *Handbook of Metaheuristics*, Springer, Boston, MA, USA, 2019.

[18] H. J. Apon, M. S. Abid, K. A. Morshed, M. M. Nishat, F. Faisal, and N. N. Ibrahim moubarak, "Power system harmonics estimation using hybrid archimedes optimization algorithm-based least Square method," in *Proceedings of the 2021 13th Int. Conf. on Info. & Comm. Tech. and System (ICTS)*, pp. 312–317, Surabaya, Indonesia, October 2021.

[19] Z. K. Eis ham, M. M. Haque, and M. S. Rahman, "Chimp Optimization Algorithm in Multilevel Image Thresholding and Image Clustering," *Evolving Systems*, 2022.

[20] F. Bayat, M. Karimi, and A. Taheri, "Robust output regulation of Zeta converter with load/input variations: LMI approach," *Control Engineering Practice*, vol. 84, pp. 102–111, 2019.

[21] S. Arun and T. Manigandan, "Design of ACO based PID controller for zeta converter using reduced order methodology," *Microprocessors and Microsystems*, vol. 81, Article ID 103629, 2021.

[22] M. Thirumeni and D. Thangavelusamy, "Design and analysis of hybrid PSO–GSA tuned PI and SMC controller for DC–DC Cuk converter," *IET Circuits, Devices and Systems*, vol. 13, pp. 374–384, 2019.

[23] Y. Sonmez, O. Ayyildiz, H. T. Kahraman, U. Guvenc, and S. Duman, "Improvement of buck converter performance using artificial bee colony optimized-PID controller," *Journal of Automation and Control Engineering*, vol. 3, pp. 304–310, 2015.

[24] P. Dhivya and K. Ranjith Kumar, "MPPT based control of SEPIC converter using firefly algorithm for solar PV system under partial shaded conditions," in *Proceedings of the 2017 International Conference on Innovations in Green Energy and Healthcare Technologies (IGEHT)*, March 2017.

[25] B. Hekimoğlu, S. Ekinci, and S. Kaya, "Optimal PID controller design of DC-DC buck converter using whale optimization algorithm," in *Proceedings of the 2018 International Conference on Artificial Intelligence and Data Processing (IDAP)*, September 2018.

[26] P. Siano and C. Citro, "Designing fuzzy logic controllers for DC–DC converters using multi-objective particle swarm optimization," *Electric Power Systems Research*, vol. 112, pp. 74–83, 2014.

[27] M. Bhuyan, D. C. Das, and A. Kumar Barik, "A comparative analysis of DSM based autonomous hybrid microgrid using PSO and SCA," in *Proceedings of the 2019 IEEE Region 10 Symposium (TENSYMP)*, June 2019.

[28] J. Águila-León, C. D. Chiñas-Palacios, C. Vargas-Salgado, E. Hurtado-Perez, and E. X. M. García, "Optimal PID parameters tunning for a DC-DC boost converter: a performance comparative using Grey Wolf optimizer, particle swarm optimization and genetic algorithms," in *Proceedings of the 2020 IEEE Conference on Technologies for Sustainability (SusTech)*, April 2020.

[29] A. Debnath, T. O. Olowu, S. Roy, I. Parvez, and A. Sarwat, "Particle swarm optimization-based PID controller design for DC-DC buck converter," in *Proceedings of the 2021 North American Power Symposium (NAPS)*, November 2021.

[30] K. Manikandan, A. Sivabalan, R. Sundar, and P. Surya, "A study of landsman, SEPIC and zeta converter by particle swarm optimization technique," in *Proceedings of the 2020 6th International Conference on Advanced Computing and Communication Systems (ICACCS)*, March 2020.

[31] A. Yadav and A. Verma, "Sepic DC–DC converter: review of different voltage boosting techniques and applications," in *Proceedings of the 2020 2nd International Conference on Innovative Mechanisms for Industry Applications (ICIMIA)*, March 2020.

[32] A. Davoudi, J. Jatskevich, and T. D. Rybel, "Numerical state-space average-value modeling of PWM DC-DC converters operating in DCM and CCM," *IEEE Transactions on Power Electronics*, vol. 21, pp. 1003–1012, 2006.

[33] S.-C. Chu, H. Hsiang-Cheh, F. R. John, and P. Jeng-Shyang, "Overview of algorithms for swarm intelligence," *International Conference on Computational Collective Intelligence*, Springer, Berlin, Heidelberg, 2011.

[34] J. A. B. Júnior, V. A. N. Marcus, H. R. N. Manoel, C. L. Jandecy, and L. M. R. Jorge, "Multi-objective optimization techniques to solve the economic emission load dispatch problem using various heuristic and metaheuristic algorithms," *Optimization and Control of Electrical Machines*, Vol. 13, IntechOpen, London, UK, 2018.

[35] S. Sheoran, N. Mittal, and A. Gelbukh, "Artificial bee colony algorithm in data flow testing for optimal test suite generation," *International Journal of System Assurance Engineering and Management*, vol. 11, pp. 340–349, 2020.

[36] Y. Xin-She, "Firefly algorithms for multimodal optimization," *Proceedings of the International symposium on stochastic algorithms*, vol. 9, pp. 169–178, Springer, Berlin, Gremnay, 2009.

[37] T. Liu, L. Liu, J. Chen, H. Jiang, Q. Sun, and Y. Xie, "Optimal design of Raman fibre amplifier based on terminal value optimization strategy and shuffled frog leaping algorithm," *Journal of Modern Optics*, vol. 65, pp. 1680–1687, 2018.

[38] A. Randazzo, "Swarm optimization methods in microwave imaging," *International Journal of Microwave Science and Technology*, pp. 1–12, 2012.

[39] S. Z. Ali, A. Ahmed Hashmani, and M. Mujtaba Shaikh, "Steady state stability analysis and improvement using eigenvalues and PSS," *Engineering, Technology & Applied Science Research*, vol. 10, pp. 5301–5306, 2020.

[40] P. Warrier and P. Shah, "Optimal fractional PID controller for buck converter using cohort intelligent algorithm," *Applied System Innovation*, vol. 4, p. 50, 2021.

[41] M. M. Nishat, F. Faisal, A. J. Evan, M. M. Rahaman, M. S. Sifat, and H. M. F. Rabbi, "Development of genetic algorithm (ga) based optimized PID controller for stability analysis of DC-DC buck converter," *Journal of Power and Energy Engineering*, vol. 8, pp. 8–19, 2020.

[42] A. Bennaoui, Slami Saadi, and A. Ameur, "Performance comparison of MFO and PSO for optimal tuning the fractional order fuzzy PID controller for A DC-DC boost converter," in *Proceedings of the 2020 International Conference on Electrical Engineering (ICEE)*, September 2020.

[43] M. Yaqoob, Z. Jianhua, F. Nawaz, T. Ali, U. Saeed, and R. Qaisrani, "Optimization in transient response of DC-DC buck converter using firefly algorithm," in *Proceedings of the 2014 16th International Conference on Harmonics and Quality of Power (ICHQP)*, May 2014.

[44] L. Chen, G. Chen, R. Wu, A. M. Lopes, J. A. Tenreiro Machado, and H. Niu, "Variable coefficient fractional-order PID controller and its application to a SEPIC device," *IET Control Theory & Applications*, vol. 14, pp. 900–908, 2020.

[45] S. Banerjee, A. Ghosh, and N. Rana, "An improved interleaved boost converter with PSO-based optimal type-III controller," *IEEE Journal of Emerging and Selected Topics in Power Electronics*, vol. 5, pp. 323–337, 2017.

[46] A. Ghosh, S. Banerjee, M. K. Sarkar, and P. Dutta, "Design and implementation of type-II and type-III controller for DC–DC switched-mode boost converter by using K-factor approach and optimisation techniques," *IET Power Electronics*, vol. 9, pp. 938–950, 2016.

[47] S. Abdelmalek, A. Dali, A. Bakdi, and M. Bettayeb, "Design and experimental implementation of a new robust observer-based nonlinear controller for DC-DC buck converters," *Energy*, vol. 213, Article ID 118816, 2020.